

Early warning of precessing compact binary merger with third-generation gravitational-wave detectors

Takuya Tsutsui,^{1,2} Atsushi Nishizawa,¹ and Soichiro Morisaki³

¹*Research Center for the Early Universe (RESCEU),
Graduate School of Science, The University of Tokyo, Tokyo 113-0033, Japan*

²*Department of Physics, Graduate School of Science,
The University of Tokyo, Tokyo 113-0033, Japan*

³*Department of Physics, University of Wisconsin-Milwaukee, Milwaukee, WI 53201, USA*

(Dated: November 13, 2020)

Rapid localization of gravitational-wave events is important for the success of the multi-messenger observations. The forthcoming improvements and constructions of gravitational-wave detectors will enable detecting and localizing compact-binary coalescence events even before mergers, which is called early warning. The performance of early warning can be improved by considering modulation of gravitational wave signal amplitude due to the Earth rotation and the precession of a binary orbital plane caused by the misaligned spins of compact objects. In this paper, for the first time we estimate localization precision in the early warning quantitatively, taking into account an orbital precession. We find that a neutron star-black hole binary at $z = 0.1$ can typically be localized to 100 deg^2 and 10 deg^2 at the time of 12 – 15 minutes and 50 – 300 seconds before merger, respectively, which cannot be achieved without the precession effect.

I. INTRODUCTION

The first joint detection of a gravitational wave (GW) and electromagnetic (EM) radiation in broad bands from binary neutron-stars (BNS) coalescence has opened a new era of multi-messenger astronomy [1, 2], which is collaborations with EM and neutrino observations. Currently the information about event triggers are shared as open public alerts, which had been used for EM follow-ups in the third observing run (O3). So far, GWs from binaries have been detected after the mergers. However, if the signals are sufficiently large, those can be detected before the mergers by accumulating enough signal-to-noise ratio (SNR), which is called early warning [3, 4]. Early warning should be important for a success of the follow-up observations and obtaining information on precursor events, prompt emission from BNS merger [5], characteristic EM emission from tidal disruption of neutron star-black hole (NSBH) [6], resonant shattering [7], fast radio burst driven by black-hole (BH) battery [8], and so on.

Until the former half of the O3, many GW events have been detected [9, 10] by advanced LIGO [11, 12] and advanced Virgo [13]. In 2030s, constructions of third-generation (3G) GW detectors, Einstein Telescope (ET) [14, 15] and Cosmic Explorer (CE) [16, 17] are planned. The 3G GW detectors are much more sensitive than advanced LIGO (see Fig. 1), and then GWs can be observed from the frequency as low as $\sim 1 \text{ Hz}$. Accordingly, the time to merger of binaries of, for example, neutron stars (NSs) with $1.4 M_\odot$ and BH with $14 M_\odot$ is $\sim 1 \text{ day}$. Since the Earth rotates at the period of one day, GWs from the binaries are modulated through the antenna response functions. In addition, the Doppler phases vary in time. These effects improve localization of the binaries at lower frequencies [18–20] and help early warning. For further improvement of the early warning,

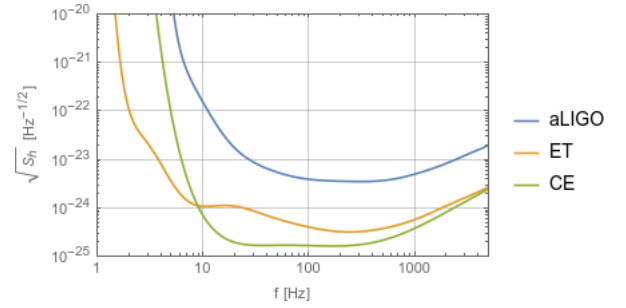


FIG. 1. Power spectral densities for advanced LIGO (blue), ET-D (orange) and CE (green).

the inclusion of higher order modes in a signal analysis has been suggested [21].

In this paper, we investigate the performance of the early warning by 3G GW detectors when precession effects of compact binaries are considered. If either or both of compact objects have non-zero misaligned spins, the total angular momentum of a binary is not parallel with the orbital angular momentum (see Fig. 2). Since, for the case, the orbital plane precesses, the amplitude of the emitted GW is modulated [22–24]. By considering the modulation, the estimation precision of binary parameters should be improved more.

The organization of this paper is as follows. In Sec. II, waveforms with precession and the Doppler phases are reviewed. In Sec. III, a Fisher analysis for the parameter estimation of early warning is reviewed. In Sec. IV, parameter estimation errors as a function of frequency or time to merger are shown. Sec. V is devoted to a summary.

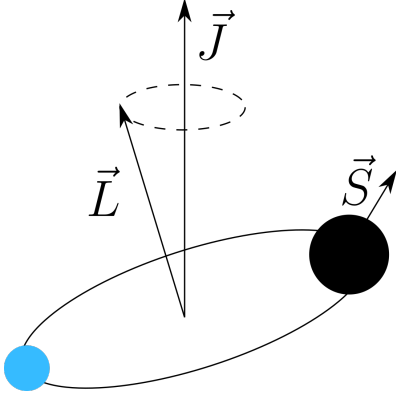


FIG. 2. Precessing binary. \vec{J} , \vec{L} and \vec{S} are respectively total, orbital and spin angular momentum.

II. WAVEFORM

Typically, a spin of a BH is much larger than that of a NS, because a spin angular momentum is proportional to mass and a BH is much heavier than a NS. Thus, even if both the components in a binary have finite spins, the spins of NSs can be neglected. To see the precession effect, a case in which a lighter component has no spin but a heavier component has non-zero spin is considered in this paper for simplicity. Variations of total and spin angular momenta, \vec{J} and \vec{S} , are at higher post-Newtonian (PN) order than the one of an orbital angular momentum, \vec{L} [22]. Then \vec{L} is precessing around \vec{J} (see Fig. 2). Considering the coordinates whose z -direction is along \vec{J} , one can deal with the precession by a rotation matrix with the Euler angles, α and β which express \vec{L} relative to \vec{J} , and ζ which expresses how much angle the component objects are rotated around \vec{L} [23, 24]. They are

$$\alpha(v) = \frac{\eta}{M} \left(2 + \frac{3m_2}{2m_1} \right) \int^v v^5 \Gamma_J \left(\frac{dv}{dt} \right)^{-1} dv, \quad (1)$$

$$\beta(v) = \cos^{-1} \left[\frac{1 + \kappa\gamma}{\Gamma_J} \right], \quad (2)$$

$$\zeta(v) = \frac{\eta}{M} \left(2 + \frac{3m_2}{2m_1} \right) \int^v v^5 (1 + \kappa\gamma) \left(\frac{dv}{dt} \right)^{-1} dv, \quad (3)$$

where

$$\gamma(v) = \frac{|\vec{S}|}{|\vec{L}|} = \frac{m_1 \chi}{m_2} v, \quad (4)$$

$$\Gamma_J(v) = \frac{|\vec{J}|}{|\vec{L}|} = \sqrt{1 + 2\kappa\gamma + \gamma^2}, \quad (5)$$

$$\kappa = \frac{\vec{L}}{|\vec{L}|} \cdot \frac{\vec{S}}{|\vec{S}|}, \quad (6)$$

m_1 and m_2 are heavier and lighter component masses, η is the symmetric mass ratio, $M = m_1 + m_2$ is the

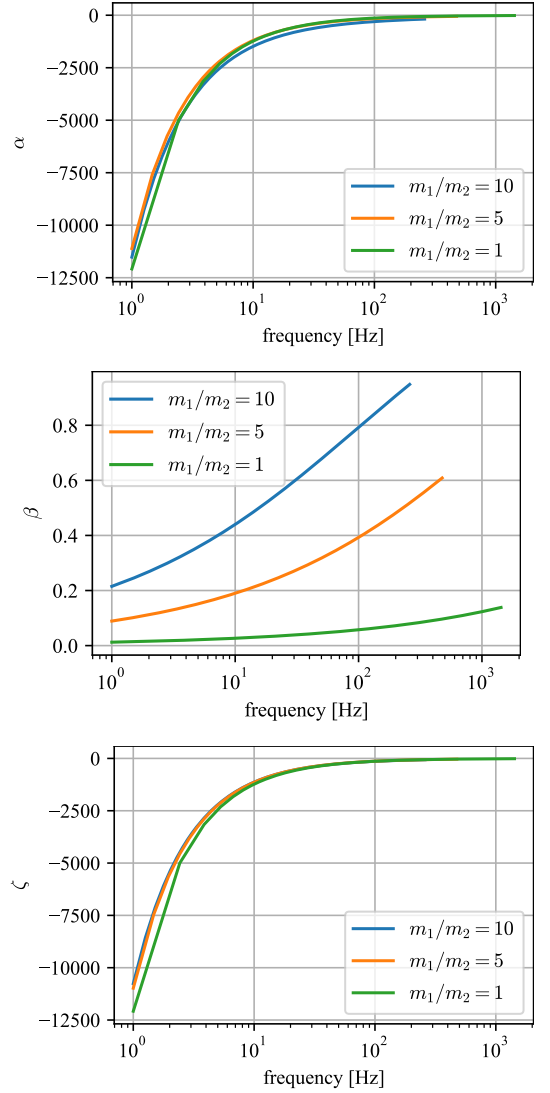


FIG. 3. Precession angles for different mass ratios as a function of frequency. The top panel is for α , the middle panel is for β , and the bottom panel is for ζ .

total mass, χ is the dimensionless spin of the primary component, and dv/dt up to 1.5PN is [25, 26]

$$\frac{dv}{dt} = \frac{32}{5} \frac{\eta}{M} v^9 \left[1 - \left(\frac{743}{336} + \frac{11}{4} \eta \right) v^2 + 4\pi v^3 \right]. \quad (7)$$

For some mass ratio, the precession angles, α , ζ , and β , are shown in Fig. 3

By using these parameters, a GW signal in the Fourier domain is

$$\tilde{h}_I(f) = Z_I(f) A(f) e^{2i(\Phi_{\text{orb}} - \zeta + \phi_{I, \text{Doppler}})}, \quad (8)$$

$$A(f) = \left(\frac{5\pi}{24} \right)^{1/2} \frac{G^2 \mathcal{M}^2}{c^5 d_L} \left(\frac{\pi G M f}{c^3} \right)^{-7/6}, \quad (9)$$

$$Z_I(f) = (C_+ F_{I,+} + C_\times F_{I,\times}) - i(S_+ F_{I,+} + S_\times F_{I,\times}) \quad (10)$$

where \mathcal{M} is the chirp mass, d_L is the luminosity distance, t_c and ϕ_c are the coalescence time and phase, $\phi_{I,\text{Doppler}}$ is the Doppler phase between the I -th detector and the

geocenter, Φ_{orb} is the orbital phase from [27, 28]. To recognize κ as constant, we neglect higher terms than 1.5PN in Φ_{orb} and use

$$\begin{aligned} \Phi_{\text{orb}} = & 2\pi f t_c - \phi_c - \pi/4 + \frac{3}{128\eta} (\pi M f)^{-5/3} \left[1 + \left(\frac{3715}{756} + \frac{55}{9}\eta \right) (\pi M f)^{2/3} \right. \\ & \left. + \left\{ -16\pi + \left(\frac{113}{3} (1 + \sqrt{1-4\eta}) - \frac{76}{3}\eta \right) \frac{\chi}{2} \right\} (\pi M f) \right]. \end{aligned} \quad (11)$$

The amplitude modulation factor for I -th detector, $Z_I(f)$, includes the antenna response functions for $+/ \times$ -modes, $F_{I,+/\times}$, and mixes them with the coefficients [24]:

$$C_+ = \frac{1}{2} \cos \theta_J [\sin^2 \alpha - \cos^2 \beta \cos^2 \alpha] + \frac{1}{2} (\cos^2 \beta \sin^2 \alpha - \cos^2 \alpha) - \frac{1}{2} \sin^2 \theta_J \sin^2 \beta - \frac{1}{4} \sin 2\theta_J \sin 2\beta \cos \alpha, \quad (12)$$

$$S_+ = \frac{1}{2} (1 + \cos^2 \theta_J) \cos \beta \sin 2\alpha + \frac{1}{2} \sin 2\theta_J \sin \beta \sin \alpha, \quad (13)$$

$$C_\times = -\frac{1}{2} \cos \theta_J (1 + \cos^2 \beta) \sin 2\alpha - \frac{1}{2} \sin \theta_J \sin 2\beta \sin \alpha, \quad (14)$$

$$S_\times = -\cos \theta_J \cos \beta \cos 2\alpha - \sin \theta_J \sin \beta \cos \alpha, \quad (15)$$

where θ_J is the inclination angle of \vec{J} . v is related to f by the Kepler's third law: $v(f) = (\pi G M f)^{1/3}$. There are many independent parameters in the GW waveform:

$$\{\lambda_i\} = \{\mathcal{M}, \eta, \chi, t_c, \phi_c, d_L, \theta, \phi, \psi, \theta_J, \kappa, \alpha_0\}, \quad (16)$$

where θ and ϕ are the longitude and latitude of a GW source, ψ is the polarization angle, and α_0 is the initial precession angle. The initial value of ζ is absorbed by ϕ_c .

Also, since the time for which a GW is observed in the bandwidth is $\mathcal{O}(1 \text{ day})$, the GW signal is modulated by the rotation of the Earth. By rotating ϕ with $\omega_E = 2\pi/(24 \text{ hours})$, one can deal with the modulation. That is, all ϕ included in Eq. (8) should be replaced with $\phi + \omega_E(t_c - t)$.

III. ANALYSIS

SNR is defined as follows:

$$\text{SNR}^2(f) = 4 \int_{f_{\min}}^f \frac{|\tilde{h}(f')|^2}{S_n(f')} df', \quad (17)$$

where $f_{\min} = 1 \text{ Hz}$ for the 3G detectors, and $S_n(f)$ is the power spectral density (see Fig. 1). Here, the maximum cutoff frequency is set to the innermost stable circular orbit (ISCO) frequency.

To compute the parameter errors, the Fisher analysis [29] is used in this paper. The Fisher matrix is defined as (i, j run over Eq. (16))

$$F'_{ij}(f) = \left(\frac{\partial h}{\partial \lambda_i} \middle| \frac{\partial h}{\partial \lambda_j} \right)_f, \quad (18)$$

$$(a|b)_f = 4\Re \int_{f_{\min}}^f \frac{\tilde{a}^*(f') \tilde{b}(f')}{S_n(f')} df'. \quad (19)$$

The Fisher analysis outputs just parameter errors, which sometimes can be too large beyond the physical ranges of parameters, for example, $\Delta\theta > 2\pi$, $\Delta\chi > 1$. This is especially for low frequencies at which information from a signal is limited, because some of the parameters are degenerated with each other and the parameter estimation does not work at all. To obtain the physically relevant errors, Gaussian priors are added as follows:

$$F_{ij}(f) = \left(\frac{\partial h}{\partial \lambda_i} \middle| \frac{\partial h}{\partial \lambda_j} \right)_f + \frac{\delta_{ij}}{(\delta\lambda_i)^2}, \quad (20)$$

where δ_{ij} is the Kronecker delta, and $\delta\lambda_i$ is a $1\text{-}\sigma$ error of a Gaussian distribution and is taken as a physical range of the parameter. By these priors, the probabilities of obtaining unphysical results decay exponentially [30]. The inverse Fisher matrix is the covariance matrix, $\Sigma = \mathbf{F}^{-1}$. Thus, the standard deviation around the true value $\Delta\lambda_i$ is

$$\Delta\lambda_i = \sqrt{\Sigma_{ii}}, \quad (21)$$

and the sky localization error $\Delta\Omega$ and error volume ΔV are given by

$$\Delta\Omega = 2\pi |\sin \theta| \sqrt{\begin{vmatrix} \Sigma_{\theta\theta} & \Sigma_{\theta\phi} \\ \Sigma_{\phi\theta} & \Sigma_{\phi\phi} \end{vmatrix}}, \quad (22)$$

$$\Delta V = \frac{4}{3}\pi |\sin \theta| \sqrt{\begin{vmatrix} \Sigma_{d_L d_L} & d_L \Sigma_{d_L \theta} & d_L \Sigma_{d_L \phi} \\ d_L \Sigma_{\theta d_L} & d_L^2 \Sigma_{\theta\theta} & d_L^2 \Sigma_{\theta\phi} \\ d_L \Sigma_{\phi d_L} & d_L^2 \Sigma_{\phi\theta} & d_L^2 \Sigma_{\phi\phi} \end{vmatrix}}. \quad (23)$$

Following the time evolution of $d_L, \Delta\Omega, \Delta V$ with $t_c - t = \frac{5}{256}(\pi f)^{-8/3}(\frac{G\mathcal{M}}{c^3})^{-5/3}$ at the Newtonian order [31, 32], the performance of early warning can be estimated.

In this paper, 200 samples are calculated for three cases of NSBH and BNS with following parameters: $z = 0.1$, $\chi = 0.5$, $\kappa = 0$, $m_2 = 1.4 M_\odot$, and $m_1 = 14 M_\odot, 7 M_\odot$ and $1.41 M_\odot$ their mass ratios are $m_1/m_2 = 10, 5$, and 1). The angles, θ and ϕ , are sampled isotropically over the sky and ψ and $\cos\theta_J$ are uniformly. It is assumed that there are one ET at the Virgo site and one CE at the Hanford site. To obtain results for other redshifts, $z \neq 0.1$, the SNR scalings in Eqs. (B1) – (B3) can be used.

IV. RESULT

In this section, we show the results of parameter estimation for NSBH with the mass ratios, $m_1/m_2 = 10$ and 5 , observed with a single detector (ET) and two detectors (ET & CE). We also compare the results with those for BNS in order to check consistency with the previous works and see how much the results change from the case of NSBH.

A. Time evolutions

Figures 4 and 5 are medians of the sky localization errors $\Delta\Omega$, the distance errors Δd_L , and the error volumes ΔV for $m_1/m_2 = 10$ and 5 , respectively. In the single detector case (ET) of Figs. 4 and 5, the precession effect much improves the localization errors at a fixed time to merger (see Table I). Furthermore, final localization errors at the time of merger are also much improved, reaching 13 Mpc, 5.7 deg^2 , and $2.5 \times 10^3 \text{ Mpc}^3$ for $m_1/m_2 = 10$ and 13 Mpc, 4.5 deg^2 , and $2.3 \times 10^3 \text{ Mpc}^3$ for $m_1/m_2 = 5$, whose volumes include 25 and 23 galaxies on average, respectively, assuming the average number density of massive galaxies, 0.01 Mpc^{-3} as in, e. g., [33]. The reason of the significant improvement for a single detector is breaking a degeneracy between the luminosity distance and the inclination angle of the orbital plane. For a non-precessing case with a single detector, even if the overall amplitude of a GW is estimated, it is difficult to separate those parameters, because the inclination angle is constant in time. In contrast, for a precessing case, the degeneracy is broken because the inclination angle is varying in time.

For double detector case (ET & CE) in Figs. 4 and 5, the results are less improved than the single detector case. However, the final errors with a precession effect reach 2.1 Mpc, 0.12 deg^2 , and 13 Mpc^3 for $m_1/m_2 = 10$ and 2.1 Mpc, 0.13 deg^2 , and 12 Mpc^3 for $m_1/m_2 = 5$, whose volumes include 0.13 and 0.12 galaxies on average and enable us to identify a unique galaxy. The reason of the less improvement for the double detector case is

because the degeneracy is already partially broken by measuring a GW with differently orientating detectors.

Variations of the samples when sky localization reaches 100 deg^2 are shown in Fig. 6. One can understand that most of events with a precession effect are detected earlier than the ones without precession: for both mass ratios, by ~ 14 minutes for the single detector case and by ~ 5 minutes for the double detector case at best. The variations of time to merger for the double detector case is smaller than that for the single detector case. This is also because the degeneracy is broken. The distributions of final errors are shown in Appendix A for readers who are interested in how widely they are scattered.

One might wonder the bends of the curves around $\sim 10^3 \text{ s}$ before merger for the double detector case. This behavior arises from the shapes of PSDs of ET and CE: ET is much more sensitive at low frequency region ($\lesssim 10 \text{ Hz}$) than CE. Then, for the low frequency range below $\sim 5 \text{ Hz}$, it is effectively the same as the single detector case even there are two detectors, ET and CE. Therefore, the precession effect is important for early warning, even if there are two 3G detectors (one is CE).

B. Comparison with previous studies

As explained in Sec. II, the spin of a NS can be neglected for high mass ratio systems. However, there is no reason to be able to do same for a BNS case. Also, for a BNS case, mass ratio is nearly unity, $\gamma(v)$ does not grow larger than a NSBH case, and then $\beta(v)$ does not, too (see Eqs. (2) and (4)). That is, a precession effect is weaker for BNS. Despite of the weakness, localization errors for the single detector case of ET are calculated to compare with the previous study (without a precession effect) [20] and to see how much the results change from the case of NSBH.

Figure 7 is the results of the sky localization error $\Delta\Omega$, the distance error Δd_L , and the error volume ΔV as a function of time to merger for the single detector case (ET). The precession effect less improves the localization errors (see Table II) and their final values due to its weakness. Especially, the final localization errors with the precession effect are 64 Mpc in distance, $1.4 \times 10^2 \text{ deg}^2$ in sky localization, $3.0 \times 10^5 \text{ Mpc}^3$ in volume, which includes 3.0×10^3 galaxies. Although there are a few differences between this study and [20] (SNR cutoff is 12 instead of 8 for this study, $d_L = 400 \text{ Mpc}$ instead of $z = 0.1$ is assumed, 500 sources instead of 200 sources, and spinless instead of non-zero precessing spin), the result is consistent with TABLE I in [20] within a factor of $\mathcal{O}(1)$, whose main origin is the spin values.

V. CONCLUSION

The constructions of 3G detectors are planned, especially ET and CE. They are sensitive to GWs from $\sim 1 \text{ Hz}$

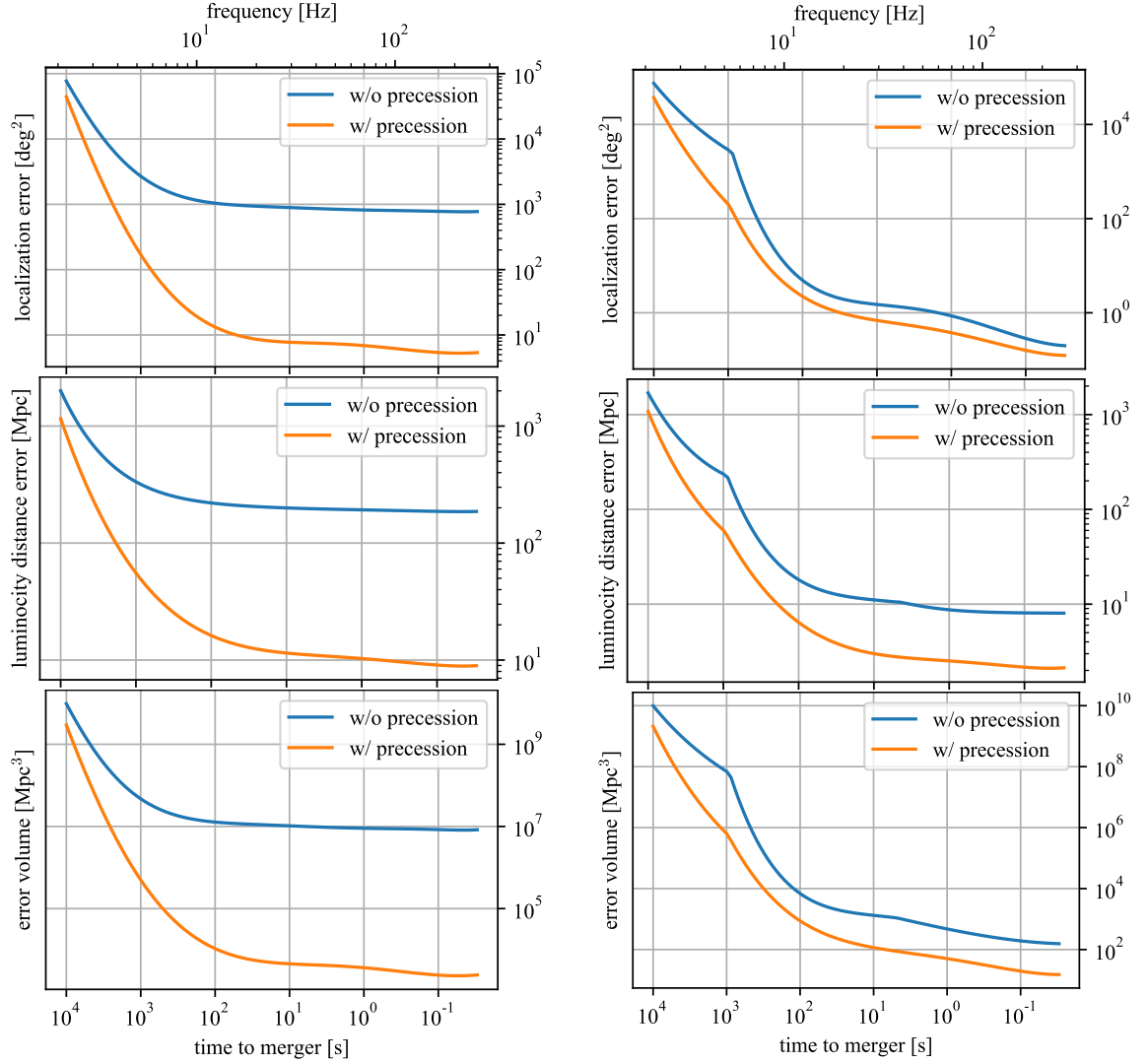


FIG. 4. Medians of localization errors for NSBH with $m_1/m_2 = 10$ as a function of time to merger. Left column is for the single detector case (ET). Right column is for the double detector case (ET & CE). From the top to the bottom, the sky localization error, the distance error, and the error volume as a function of time to merger. Blue (Orange) lines are without (with) a precession effect.

or ~ 1 day before mergers. In this case, one can consider the modulation of a GW signal by the Earth rotation and a precession effect for NSBH. In this paper, for the first time we estimate how much the performance of early warning is improved by considering the precession effect together with the Earth rotation.

By considering precession, since the degeneracy between the inclination angle and the luminosity distance is broken, the performance of early warning is much improved for the single detector case (see Table I, Fig. 4 and Fig. 5). For the double detector case, because the degeneracy is already partially broken by measuring a GW with differently orientating detectors, the performance of early warning is less improved from the case without the precession effect (see Table I, Fig. 4 and Fig. 5). Despite of the double detector case, it is effectively the single detector case for low frequencies below ~ 5 Hz due to the

difference of the power spectral densities between ET and CE (see Fig. 1). This is the reason of inhomogeneous improvement of the performance in each frequency range for the double detector case.

In conclusion, the precession effect is very useful for the early warning, especially, when only one detector is in an observing mode. Even if two detectors are in the observing modes, the precession effect modestly improves the performance of early warning. Importantly, the precision of the sky localization can reach 100 deg^2 and 10 deg^2 at the time of 12 – 15 minutes and 50 – 300 seconds before merger, respectively. These small localization areas enable us to search an EM counterpart within the fields of view of EM telescopes, for example, Cherenkov telescope array (CTA) [34, 35] ($\sim 70 \text{ deg}^2$), Swift-BAT [36] ($\sim 4600 \text{ deg}^2$), Fermi-LAT [37] ($\sim 7900 \text{ deg}^2$), and LSST [38] ($\sim 9.6 \text{ deg}^2$).

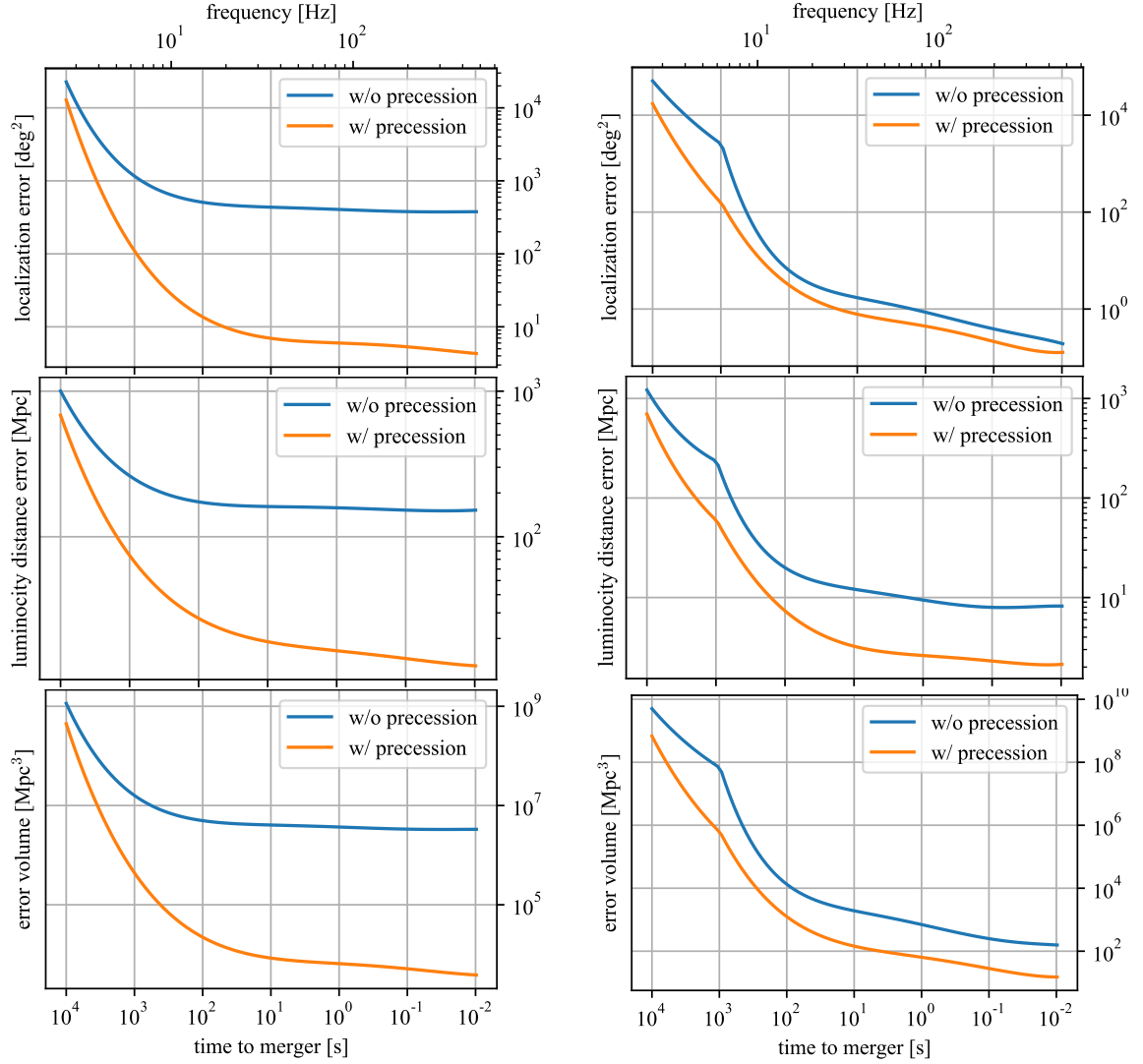


FIG. 5. The same as Fig. 4 but for $m_1/m_2 = 5$.

ACKNOWLEDGMENTS

T. T. is supported by International Graduate Program for Excellence in Earth-Space Science (IGPEES). A. N. is supported by JSPS KAKENHI Grant Nos. JP19H01894 and JP20H04726 and by Research Grants from Inamori Foundation. S. M. is supported by JSPS KAKENHI Grant Number 19J13840.

Appendix A: Final Error Distributions

Figure 8 is the distributions of SNR and the localization errors at the merger (up to the ISCO frequency) for NSBH with $m_1/m_2 = 10$ samples calculated in Sec. IV. The left panels are for the single detector case, and the right panels are for the double detectors case. Figure 9 is the distributions for BNS. Blue histograms are for non-precessing case, and orange histograms are for a precess-

ing case.

When binaries are precessing, the inclination angle does not stay in a certain direction that GW amplitude becomes larger or smaller. Thus the variation of SNR for NSBH becomes smaller when precession is considered, because the precession effect is stronger for NSBH than for BNS. The localization errors, $\Delta\Omega$ and $\Delta d_L/d_L$, for NSBH and BNS are improved by including the precession effect.

Appendix B: SNR scalings

Errors estimated by the Fisher analysis scale with respect to SNR [29]:

$$\Delta d_L \propto \text{SNR}^{-1}, \quad (\text{B1})$$

$$\Delta\Omega \propto \text{SNR}^{-2}, \quad (\text{B2})$$

$$\Delta V \propto \text{SNR}^{-3}. \quad (\text{B3})$$

TABLE I. Time to merger for NSBH with some conditions from Figs. 4 and 5. The number density of massive galaxies assumed is 0.01 Mpc^{-3} .

detector		time to merger [s]			
		$m_1/m_2 = 10$		$m_1/m_2 = 5$	
		w/o precession	w/ precession	w/o precession	w/ precession
ET	$\Delta\Omega = 1000 \text{ deg}^2$	71	2.4×10^3	7.9×10^2	3.6×10^3
	$\Delta\Omega = 100 \text{ deg}^2$	-	7.3×10^2	-	9.3×10^2
	$\Delta\Omega = 10 \text{ deg}^2$	-	52	-	49
	$\Delta V = 10^7 \text{ Mpc}^3$ (10^5 galaxy)	6.2	2.6×10^3	5.7×10^2	3.5×10^3
	$\Delta V = 10^5 \text{ Mpc}^3$ (10^3 galaxy)	-	5.1×10^2	-	4.2×10^2
	$\Delta V = 10^4 \text{ Mpc}^3$ (10^2 galaxy)	-	93	-	20
ET & CE	$\Delta\Omega = 100 \text{ deg}^2$	4.1×10^2	7.8×10^2	4.2×10^2	8.2×10^2
	$\Delta\Omega = 10 \text{ deg}^2$	1.6×10^2	3.0×10^2	1.4×10^2	2.5×10^2
	$\Delta\Omega = 1 \text{ deg}^2$	1.5	31	1.6	20
	$\Delta V = 10^5 \text{ Mpc}^3$ (10^3 galaxy)	2.8×10^2	6.3×10^2	2.4×10^2	6.1×10^2
	$\Delta V = 10^4 \text{ Mpc}^3$ (10^2 galaxy)	1.2×10^2	3.1×10^2	83	2.8×10^2
	$\Delta V = 10^3 \text{ Mpc}^3$ (10^1 galaxy)	4.1	1.1×10^2	2.2	86

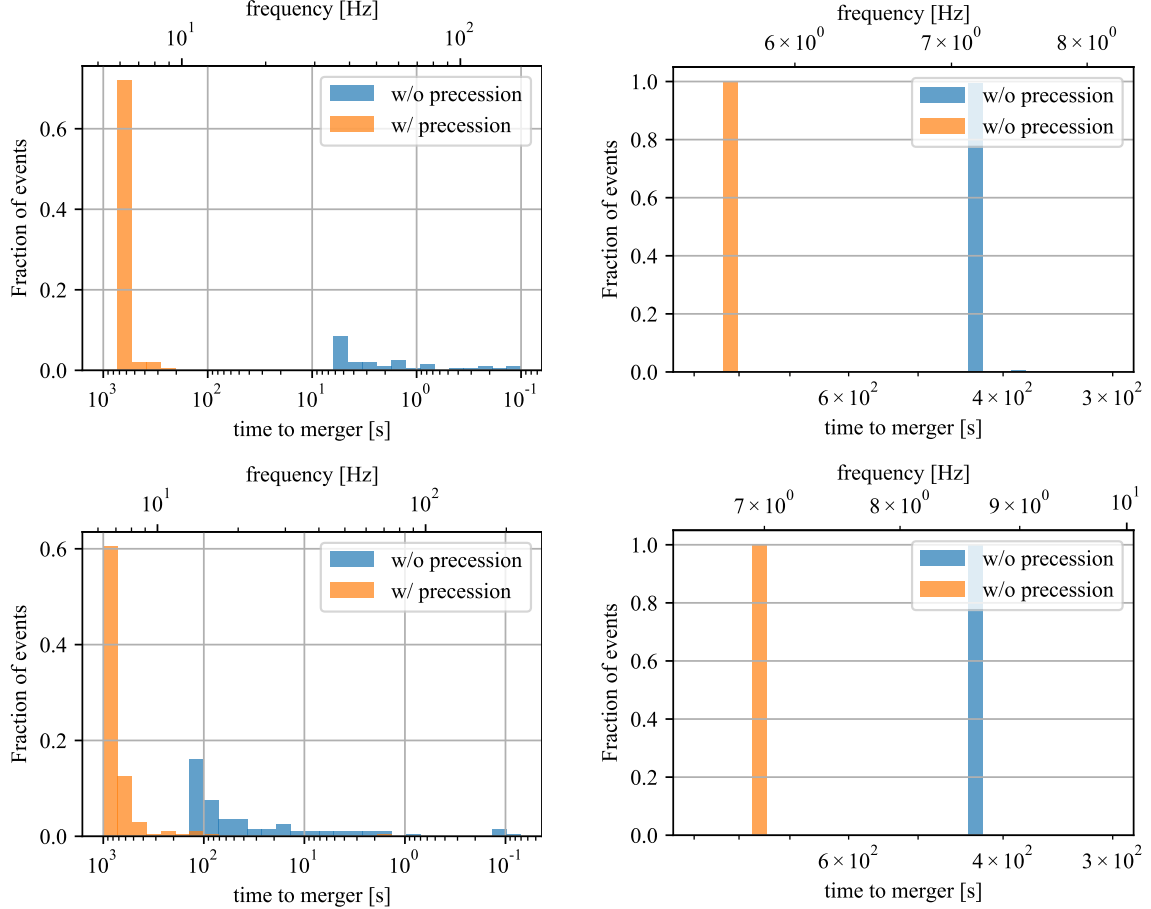


FIG. 6. Distributions of time to merger of detectable events when sky localization reaches 100 deg^2 for NSBH with $m_1/m_2 = 10$ (top) and 5 (bottom). Left column is for the single detector case (ET). Right one is for the double detector case (ET & CE).

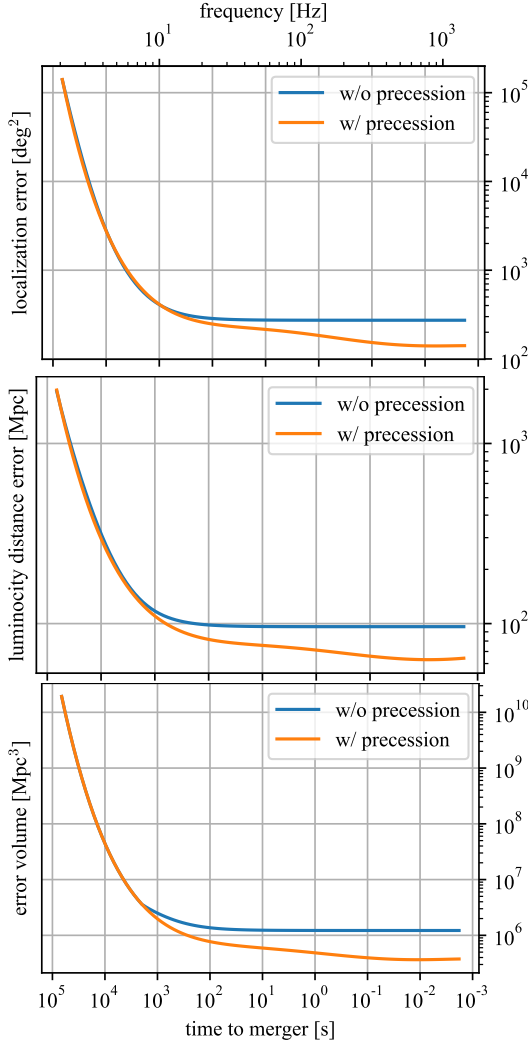


FIG. 7. Medians of localization errors for BNS in the single detector case (ET) as a function of time to merger. From the top to the bottom, the sky localization error, the distance error, and the error volume as a function of time to merger. Blue (Orange) lines are without (with) the precession effect.

TABLE II. Time to merger for BNS with some conditions from Fig. 7. The Earth rotation is considered. A density of galaxies is 0.01 Mpc^{-3} [33].

detector		time to merger [s]	
		w/o precession	w/ precession
ET	$\Delta\Omega = 1000 \text{ deg}^2$	4.2×10^3	4.2×10^3
	$\Delta\Omega = 700 \text{ deg}^2$	2.8×10^3	2.8×10^3
	$\Delta\Omega = 400 \text{ deg}^2$	9.4×10^2	9.4×10^2
	$\Delta V = 10^7 \text{ Mpc}^3$	4.4×10^3	4.4×10^3
	(10^5 galaxy)		
	$\Delta V = 6 \times 10^6 \text{ Mpc}^3$	3.1×10^3	3.1×10^3
	(6×10^4 galaxy)		
	$\Delta V = 2 \times 10^6 \text{ Mpc}^3$	5.8×10^2	1.0×10^3
	(6×10^4 galaxy)		

¹ If $\alpha(v) = \pi$, the phase is $\beta + \theta_J$ instead of $\beta - \theta_J$. The phase in

For sources at redshifts other than $z = 0.1$, all the errors estimated in this paper basically scale by the relations above, though the range of the frequency integral is slightly modified because of the redshift.

However, for sources at a fixed redshift but with different precession parameters, the SNR scalings are non-trivial and do not hold in the single detector case. The estimated errors for NSBH with $m_1/m_2 = 10$ are shown as a function of SNR in Fig. 10. The sky localization errors in the single detector case do not simply decrease as the SNR increases. For a non-precessing case, the errors are highly scattered, indicating that the degeneracies between the extrinsic parameters exist. For a precessing case, the localization errors scale with SNR even inversely. These can be understood as follows. GW amplitude is proportional to the norm of Eq. (10), which oscillates by the change of α . Neglecting the oscillation, that is, setting $\alpha(v) = 0$, the norm is smoothly changed by β ¹:

$$|Z|^2|_{\alpha=0} = F_{\times}^2 \cos^2(\beta - \theta_J) + \frac{1}{16} F_{+}^2 \{3 + \cos 2(\beta - \theta_J)\}^2, \quad (\text{B4})$$

which is plotted as a function of $\beta - \theta_J$ in Fig. 11. Since $\beta(v)$ increases as time goes, $|Z|^2$ decreases if $\beta - \theta_J$ starts from ~ 0 or π at low frequencies and increases if it starts from $\sim \pi/2$. As SNR is more earned at lower frequencies and the localization errors, $\Delta\Omega$ and $\Delta d_L/d_L$, are mostly determined at higher frequencies, where GW amplitude is larger and a timing error is $\sim 1/f$, high (low) SNR events have smaller (larger) GW amplitude at high frequencies and give worse (better) localization errors. Thus, the errors of the extrinsic parameters increase with respect to SNR. The physical interpretation for the inverse SNR scalings is that tilting \vec{L} from \vec{J} as time evolves, and then the flux of GW to observer increase or decrease depending on the initial inclination. Thus the inverse SNR scaling is just a bias when a redshift is fixed.

The double detector case obeys a normal scaling with SNR, because the degeneracies between the inclination and other extrinsic parameters are almost broken by measuring GWs with different orientating detectors.

the cosine functions is the angle between \vec{L} and the line of sight.

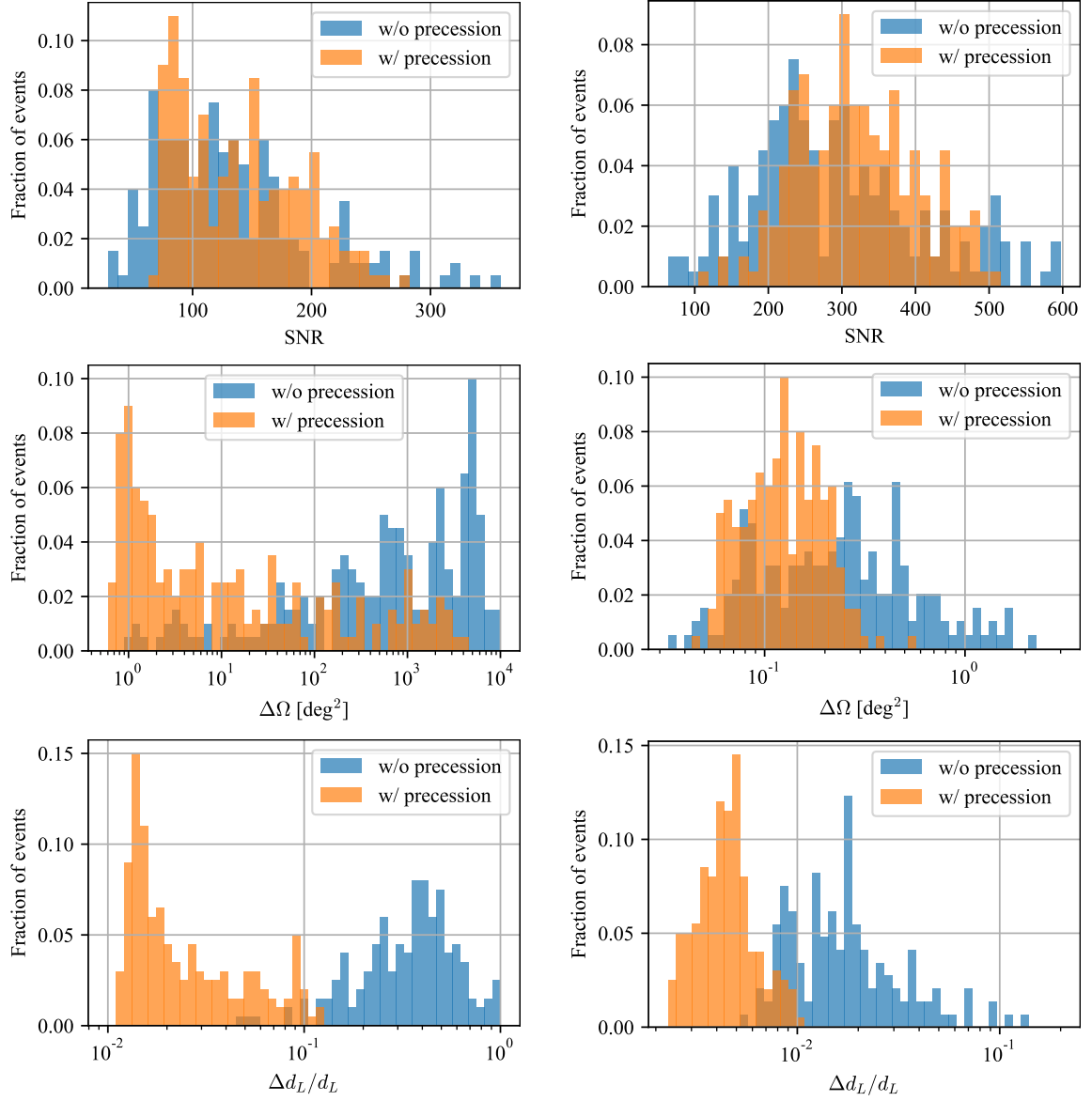


FIG. 8. Distributions of SNR (top), $\Delta\Omega$ (middle) and $\Delta d_L/d_L$ (bottom) for NSBH with $m_1/m_2 = 10$. Left column is for the single detector case (ET). Right one is for the double detector case (ET & CE).

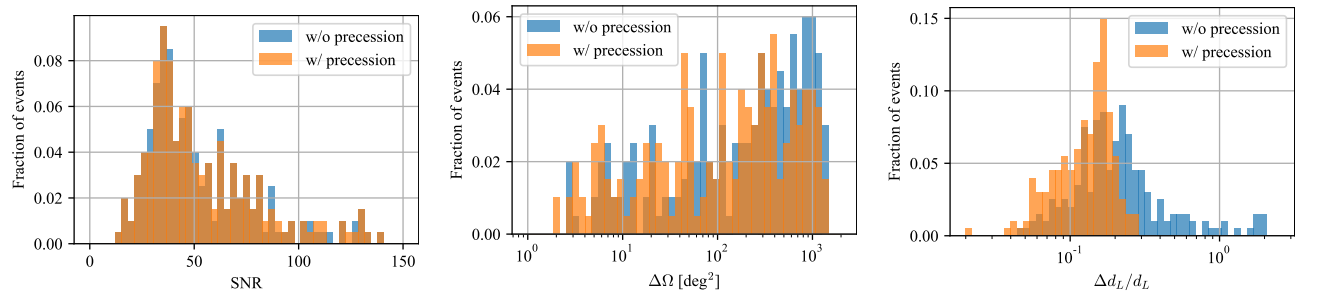


FIG. 9. Distributions of SNR (left), $\Delta\Omega$ (middle) and $\Delta d_L/d_L$ (right) for BNS.

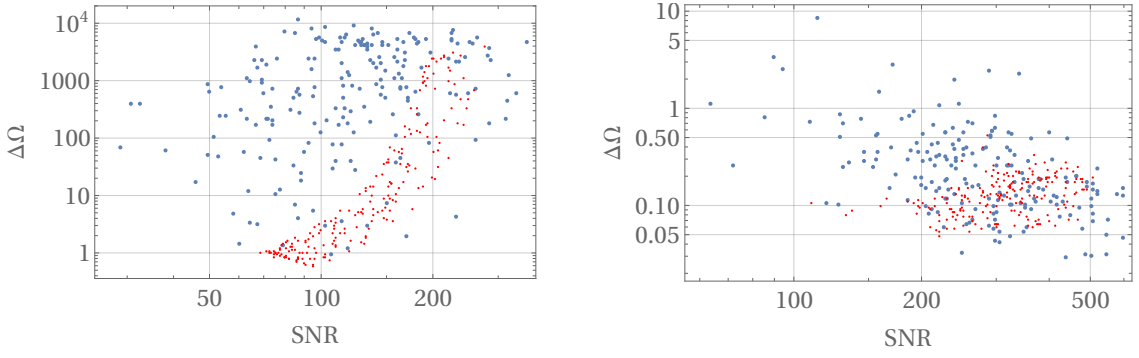


FIG. 10. SNR dependences of sky localization errors for NSBH with $m_1/m_2 = 10$. Left panel is for single detector case, whereas Right panel is for double detectors case. Blue (Red) dots are with the earth rotation without (with) precession effect.

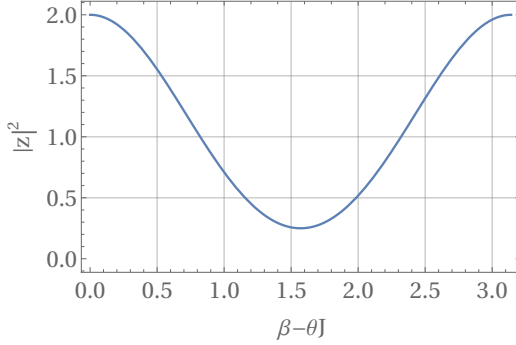


FIG. 11. $\beta - \theta_J$ vs $|Z|^2$ for $\alpha(v) = 0, F_- = 0, F_+ = 1$.

-
- [1] B. P. Abbott, R. Abbott, T. D. Abbott, F. Acernese, K. Ackley, C. Adams, T. Adams, P. Addesso, R. X. Adhikari, V. B. Adya, and et al. GW170817: Observation of Gravitational Waves from a Binary Neutron Star Inspiral. *Physical Review Letters*, 119(16), Oct 2017.
 - [2] B. P. Abbott et al. Multi-messenger Observations of a Binary Neutron Star Merger. *Astrophys. J.*, 848(2):L12, 2017.
 - [3] Kipp Cannon and Romain Carriu et al. TOWARD EARLY-WARNING DETECTION OF GRAVITATIONAL WAVES FROM COMPACT BINARY COALESCENCE. *The Astrophysical Journal*, 748(2):136, Mar 2012.
 - [4] Surabhi Sachdev and Ryan Magee et al. An early warning system for electromagnetic follow-up of gravitational-wave events, 2020.
 - [5] Ehud Nakar. Short-hard gamma-ray bursts. *Physics Reports*, 442(1):166 – 236, 2007. The Hans Bethe Centennial Volume 1906-2006.
 - [6] Sean T. McWilliams and Janna Levin. ELECTROMAGNETIC EXTRACTION OF ENERGY FROM BLACK-HOLE-NEUTRON-STAR BINARIES. *The Astrophysical Journal*, 742(2):90, Nov 2011.
 - [7] David Tsang, Jocelyn S. Read, Tanja Hinderer, Anthony L. Piro, and Ruxandra Bondarescu. Resonant Shattering of Neutron Star Crusts. *Phys. Rev. Lett.*, 108:011102, Jan 2012.
 - [8] Chiara M. F. Mingarelli, Janna Levin, and T. Joseph W. Lazio. FAST RADIO BURSTS AND RADIO TRANSIENTS FROM BLACK HOLE BATTERIES. *The Astrophysical Journal*, 814(2):L20, nov 2015.
 - [9] B. P. Abbott, R. Abbott, T. D. Abbott, S. Abraham, F. Acernese, K. Ackley, C. Adams, R. X. Adhikari, V. B. Adya, C. Affeldt, and et al. GWTC-1: A Gravitational-Wave Transient Catalog of Compact Binary Mergers Observed by LIGO and Virgo during the First and Second Observing Runs. *Physical Review X*, 9(3), Sep 2019.
 - [10] R. Abbott, T. D. Abbott, and et al. GWTC-2: Compact Binary Coalescences Observed by LIGO and Virgo During the First Half of the Third Observing Run, 2020.
 - [11] J Aasi, B P Abbott, R Abbott, T Abbott, M R Abernathy, K Ackley, C Adams, T Adams, P Addesso, and et al. Advanced LIGO. *Classical and Quantum Gravity*, 32(7):074001, Mar 2015.
 - [12] Gregory M Harry. Advanced LIGO: the next generation of gravitational wave detectors. *Classical and Quantum Gravity*, 27(8):084006, apr 2010.
 - [13] F Acernese, M Agathos, K Agatsuma, D Aisa, N Allemandou, A Allocca, J Amarni, P Astone, G Balestri, G Ballardin, and et al. Advanced Virgo: a second-generation interferometric gravitational wave detector. *Classical and Quantum Gravity*, 32(2):024001, Dec 2014.
 - [14] M Punturo et al. The Einstein Telescope: a third-generation gravitational wave observatory. *Classical and*

- Quantum Gravity*, 27(19):194002, sep 2010.
- [15] Michele Maggiore, Chris Van Den Broeck, Nicola Bartolo, Enis Belgacem, Daniele Bertacca, Marie Anne Bizouard, Marica Branchesi, Sebastien Clesse, Stefano Foffa, Juan García-Bellido, and et al. Science case for the Einstein telescope. *Journal of Cosmology and Astroparticle Physics*, 2020(03):050–050, Mar 2020.
 - [16] B P Abbott and et al. Exploring the sensitivity of next generation gravitational wave detectors. *Classical and Quantum Gravity*, 34(4):044001, jan 2017.
 - [17] Sheila Dwyer, Daniel Sigg, Stefan W. Ballmer, Lisa Barsotti, Nergis Mavalvala, and Matthew Evans. Gravitational wave detector with cosmological reach. *Phys. Rev. D*, 91:082001, Apr 2015.
 - [18] Wen Zhao and Linqing Wen. Localization accuracy of compact binary coalescences detected by the third-generation gravitational-wave detectors and implication for cosmology. *Phys. Rev. D*, 97:064031, Mar 2018.
 - [19] Atsushi Nishizawa and Shun Arai. Generalized framework for testing gravity with gravitational-wave propagation. III. Future prospect. *Phys. Rev. D*, 99:104038, May 2019.
 - [20] Man Leong Chan, Chris Messenger, Ik Siong Heng, and Martin Hendry. Binary neutron star mergers and third generation detectors: Localization and early warning. *Phys. Rev. D*, 97:123014, Jun 2018.
 - [21] Shasvath J. Kapadia, Mukesh Kumar Singh, Md Arif Shaikh, Deep Chatterjee, and Parameswaran Ajith. Of Harbingers and Higher Modes: Improved Gravitational-wave Early Warning of Compact Binary Mergers. *The Astrophysical Journal*, 898(2):L39, jul 2020.
 - [22] Theocharis A. Apostolatos, Curt Cutler, Gerald J. Sussman, and Kip S. Thorne. Spin-induced orbital precession and its modulation of the gravitational waveforms from merging binaries. *Phys. Rev. D*, 49:6274–6297, Jun 1994.
 - [23] Andrew Lundgren and R. O’Shaughnessy. Single-spin precessing gravitational waveform in closed form. *Phys. Rev. D*, 89:044021, Feb 2014.
 - [24] Duncan A. Brown, Andrew Lundgren, and R. O’Shaughnessy. Nonspinning searches for spinning black hole-neutron star binaries in ground-based detector data: Amplitude and mismatch predictions in the constant precession cone approximation. *Phys. Rev. D*, 86:064020, Sep 2012.
 - [25] Alessandra Buonanno, Bala R. Iyer, Evan Ochsner, Yi Pan, and B. S. Sathyaprakash. Comparison of post-Newtonian templates for compact binary inspiral signals in gravitational-wave detectors. *Phys. Rev. D*, 80:084043, Oct 2009.
 - [26] Alexander H. Nitz, Andrew Lundgren, Duncan A. Brown, Evan Ochsner, Drew Keppel, and Ian W. Harry. Accuracy of gravitational waveform models for observing neutron-star-black-hole binaries in Advanced LIGO. *Phys. Rev. D*, 88:124039, Dec 2013.
 - [27] Sascha Husa, Sebastian Khan, Mark Hannam, Michael Pürrer, Frank Ohme, Xisco Jiménez Forteza, and Alejandro Bohé. Frequency-domain gravitational waves from nonprecessing black-hole binaries. I. New numerical waveforms and anatomy of the signal. *Phys. Rev. D*, 93:044006, Feb 2016.
 - [28] Sebastian Khan, Sascha Husa, Mark Hannam, Frank Ohme, Michael Pürrer, Xisco Jiménez Forteza, and Alejandro Bohé. Frequency-domain gravitational waves from nonprecessing black-hole binaries. II. A phenomenological model for the advanced detector era. *Phys. Rev. D*, 93:044007, Feb 2016.
 - [29] Curt Cutler and Éanna E. Flanagan. Gravitational waves from merging compact binaries: How accurately can one extract the binary’s parameters from the inspiral waveform? *Phys. Rev. D*, 49:2658–2697, Mar 1994.
 - [30] L. Verde. Statistical Methods in Cosmology. *Lecture Notes in Physics*, page 147–177, 2010.
 - [31] M. Maggiore. *Gravitational Waves: Volume 1: Theory and Experiments*. Gravitational Waves. OUP Oxford, 2008.
 - [32] Jolien D. E. (Jolien Donald Earl) Creighton and Warren G. Anderson. *Gravitational-wave physics and astronomy : an introduction to theory, experiment and data analysis*. Wiley-VCH, 2011.
 - [33] Atsushi Nishizawa. Measurement of Hubble constant with stellar-mass binary black holes. *Phys. Rev. D*, 96:101303, Nov 2017.
 - [34] Takuya Tsutsui, Kipp Cannon, and Leo Tsukada. High Speed Source Localization in Searches for Gravitational Waves from Compact Object Collisions, 2020.
 - [35] A. Acharyya et al. Monte Carlo studies for the optimisation of the Cherenkov Telescope Array layout. *Astropart. Phys.*, 111:35–53, 2019.
 - [36] Scott D. Barthelmy, Louis M. Barbier, Jay R. Cummings, Ed E. Fenimore, Neil Gehrels, Derek Hullinger, Hans A. Krimm, Craig B. Markwardt, David M. Palmer, Ann Parsons, and et al. The Burst Alert Telescope (BAT) on the SWIFT Midex Mission. *Space Science Reviews*, 120(3-4):143–164, Oct 2005.
 - [37] W. B. Atwood, A. A. Abdo, M. Ackermann, W. Althouse, B. Anderson, M. Axelsson, L. Baldini, J. Ballet, D. L. Band, G. Barbiellini, and et al. THE LARGE AREA TELESCOPE ON THE FERMI GAMMA-RAY SPACE TELESCOPE MISSION. *The Astrophysical Journal*, 697(2):1071–1102, May 2009.
 - [38] Željko Ivezić, Steven M. Kahn, J. Anthony Tyson, Bob Abel, Emily Acosta, Robyn Allsman, David Alonso, Yusra AlSayyad, Scott F. Anderson, John Andrew, and et al. LSST: From Science Drivers to Reference Design and Anticipated Data Products. *The Astrophysical Journal*, 873(2):111, Mar 2019.